Arterial Wall Motion Estimation in Carotid Artery Using Deep Learning with Extended Kalman Filter

S. Bharawdaj and M. Almekkawy

School of Elect. Eng. and Comp. Sci., The Pennsylvania State University, University Park, PA, USA
{ssb248, mka9}@psu.edu

Abstract— Arterial wall motion estimation of the carotid artery is known to be extremely useful in the diagnosis of atherosclerotic diseases. While several approaches have been developed for robust tracking of the arterial wall, real-time tracking for hand-held devices remains a challenging task. Towards this end, we propose a deep learning-based tracker with a non-linear motion model describing the dynamics of the arterial wall. The proposed model uses a Siamese architecture-based convolutional neural network for detection and a non-linear motion model that incorporates an Extended Kalman Filter. Initial experiments proved that the proposed model works in near real-time with promising tracking accuracy when compared with conventional techniques such as exhaustive search-based similarity matching.

I. INTRODUCTION

Motion tracking in ultrasound sequences is proving to be extremely useful in several applications such as liver ultrasound tracking [1], shear wave elastography [2] and echocardiography [3]. Motion estimation in ultrasound images has been proven to be extremely useful. Numerous robust object tracking techniques have been proposed [4]. These techniques include traditional image tracking techniques such as block matching [5], optical flow [6], correlation filters [7] and multi-dimensional speckle tracking [8–13] . Modern motion estimation techniques include Convolutional Neural Networks (CNN)-based techniques such as Flownet [14], GLUENet [15], and Siamese architecture-based networks [16–19].

Motion estimation using similarity matching typically involves detecting a predefined region of interest (ROI), called the reference block, through all the frames of an image sequence by searching through each frame exhaustively and comparing the reference block with candidate blocks using a cost function such as Mean Absolute Difference (MAD), Mean Squared Error (MSE), Normalized Cross Correlation (NCC) [20]. While alternative algorithms to improve the speed of search have also been introduced [21], exhaustive search is heavily used in ultrasound images in the context of similarity matching. However, it is well-known that exhaustive search can be extremely slow for real-time devices. Furthermore, CNN-based techniques involve a similar strategy, in which CNNs are used to detect the given reference ROI. Siamese architectures-based networks are well-known for similarity matching and are being heavily borrowed into the medical applications for mo-

tion estimation. In this paper, a Siamese network called the Fully-Convolutional Siamese Network (SiamFC) [22] is used to track ROIs in ultrasound images. In [17], authors proved that CNNs alone might not be sufficient for robust motion tracking and additional modules such as motion models and frame anchoring-based reference block update are required for accurate tracking. In this paper, we attempt to track the arterial wall of the carotid artery using a Siamese network along with a non-linear motion model that closely describes the arterial wall motion.

Early diagnosis is of vital importance to prevent mortality due to atherosclerotic diseases. In the diagnosis of atherosclerotic diseases, the arterial wall motion of the carotid artery can be considered as an independent predictor [23]. Nevertheless, the challenges posed by the ultrasound images such as air-shadowing, insufficient distinction between background and foreground demand got a robust and accurate motion estimation technique. In this paper, we try to address the issue using SiamFC along with frame anchoring-based reference block update and an non-linear motion model. The non-linear motion model is inspired by the dynamics of the Van der Pol oscillator that closely follows the dynamics of the arterial wall motion of the carotid artery. The non-linear motion model is incorporated using an EKF. In addition, we proved that the proposed model has higher tracking accuracy and computational speed compared to the traditional exhaustive search-based similarity matching (ES-SM) technique.

II. METHODOLOGY

Our proposed model (SiamFC-EKF) considers the exact network presented in [22]. In addition to this network, frame anchoring-based template update and a motion model is introduced into our model as presented in our associated paper [17]. In this section, we present a brief description of SiamFC and the template update and detailed explanation of the aforementioned non-linear motion model.

II-A. Siamese Architecture

Siamese architecture-based network consists of two parallel CNNs. While one of the networks extracts the features of the reference block, the other one is used to extract features of the candidate blocks in subsequent frames. Fig. 1 represents the SiamFC described in [22]. In this architecture, the network is fully-convolutional
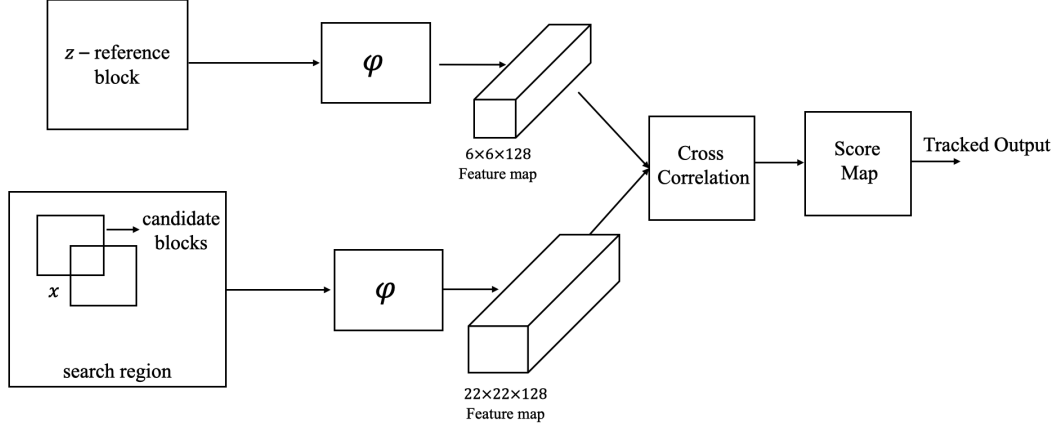
Figure 1. Siamese architecture

in that there are no fully connected layers. With this architecture two images of different sizes can be input to the Siamese network. Thus, we can input a larger image x within which the reference block z can be searched. The network is then allowed to learn a function $f(z,x)$, that compares the similarity between the reference block z and the candidate blocks within x. Once $f(z,x)$ is learnt, the network outputs a high score when the two blocks are similar and a low score if not. Since x consists of several candidate blocks, the network outputs a score map and not just a single value. Once the score map is obtained, the tracked output is selected by identifying the candidate block with the highest score. This technique is advantageous in that once the network is trained, it avoids the calculation of the cost function in every iteration for comparison. Thus, the network inherently becomes computationally less expensive compared to the traditional ES-SM technique. On the other hand, the original SiamFC, by itself, is not robust due to the inherent limitations. First, the original architecture does not consider reference block update. Hence, the network is sensitive against deform-

ing objects. Second, a motion model is not considered as a part of the network. Therefore, the tracked outputs are merely detections obtained from the CNN. These limitations were addressed in our associated paper [17]. To overcome the aforementioned limitations we used frame anchoring-based reference block update to ensure that the architecture is robust against deforming objects and adopted a linear motion model using a Linear Kalman Filter (LKF). The performance of the model was tested exhaustively on a publicly curated data set [1]. Fig. 2 represents the model proposed in [17]. In this paper, we use a non-linear motion model within the motion model block to predict the movement of the arterial wall and an EKF within the Kalman Filter block to merge predictions and measurements. We describe the two models in the following subsections.

II-B. Frame anchoring-based Template Update

One of the major limitations of the SiamFC is that the network considers a constant position model. That is, the reference object is assumed to not deform through the subsequent frames of the image sequence. Thus, the network is sensitive to deformations in the region of interest. This is an inherent limitation of the original model. In order to overcome this limitation, we allow a conditional update on the reference block based on the output of the Kalman filter. We allow the reference block to update with the latest tracked output if the reference block and the tracked output have a correlation coefficient (G) beyond a predefined threshold.

$$G = \frac{\sum_i \sum_j (z_{ij} - \bar{z})(x_{ij}^m - \bar{x}^m)}{\sqrt{\sum_i \sum_j (z_{ij} - \bar{z})^2}\sqrt{\sum_i \sum_j (x_{ij}^m - \bar{x}^m)^2}} \quad (1)$$

Let z be the reference block and x^m be the tracked output (m^{th} candidate block within x is chosen to be the output by the detection module) in a given frame. The coefficient score between the two blocks is found using the Eq. (1)[17].
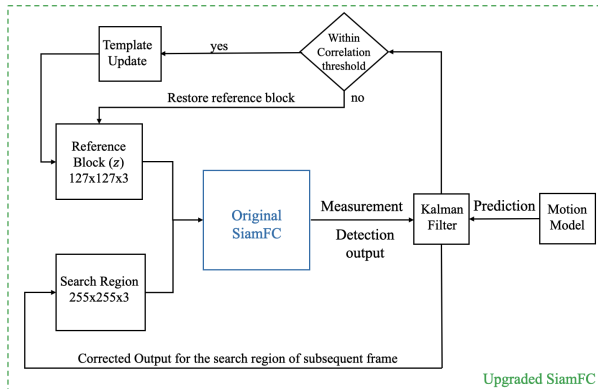

Figure 2. Schematic of the upgraded Siamese network. In this paper, a non-linear motion model is used and is incorporated with an EKF.

II-C. Non-linear Motion Model using Extended Kalman Filter

The motion model of the carotid artery is assumed to satisfy the following state-space equation:

$$\mathbf{x_{k+1}} = f(\mathbf{x_k}, \mathbf{u_k}) + \mathbf{n_k} \quad \mathbf{z_k} = h(\mathbf{x_k}) + \mathbf{v_k} \tag{2}$$

where, k is the frame index, $\mathbf{x_k}$ is the current state at frame k, $\mathbf{z_k}$ represents the observation of the state at frame k. $\mathbf{n_k}$ and $\mathbf{v_k}$ represent the process and measurement noise, respectively. Both $\mathbf{n_k}$ and $\mathbf{v_k}$ are zero mean Gaussian noise represented as $\mathbf{n_k} \ \mathcal{N}(0, \mathbf{Q})$ and $\mathbf{n_k} \ \mathcal{N}(0, \mathbf{C})$. $\mathbf{Q}$ and $\mathbf{C}$ represent the process and measurement covariance matrices for which, the values are set to $q\mathbf{I}$ and $c\mathbf{I}$, respectively. Based on our experiments, the covariance constants q and c were set to $q = 6$ and $c = 2$.

In this paper, the state equations and control equations resemble the equations used in [20]. The state $\mathbf{x_k}$ is defined as the centroid location ($\mathbf{x_k} = [x_k, y_k]^T$) of the reference block, where x_k and y_k represent x-coordinate and y-coordinate of the centroid, respectively. The f represents the motion of the Van der Pol oscillator. Eq. (3) represents the state equation governing the coordinates of the centroid

$$x_k = x_{k-1} - \frac{T}{5} y_{k-1} + T u_1$$
$$y_k = (1 - \frac{T}{5}) y_{k-1} + T x_{k-1} - \frac{T}{373} x_{k-1} y_{k-1} + T u_2 \tag{3}$$

where, T is the sampling period. The control signal $\mathbf{u_k} = [u_1, u_2]^T = g_1(k) + g_2(k)$ is based on the mathematical model [24, 25] represented in Eq. (4). Our motion model resembles the model presented in [20] by Gao et al. By linearizing Eq. (4), the state equation and measurement equations are modelled as

$$\mathbf{x_k} = \mathbf{F x_{k-1}} + \mathbf{B u_k} + \mathbf{n_k}$$
$$\mathbf{z_k} = \mathbf{H x_k} + \mathbf{v_k} \tag{5}$$

where, $\mathbf{F}$ is the state transition matrix defined as,

$$\mathbf{F} = \begin{bmatrix} 1 & -dt/5 \\ dt - (\frac{dt}{373} y_k) & (1 - \frac{dt}{5}) - (\frac{dt}{373} x_k) \end{bmatrix} \tag{6}$$

and the control matrix $\mathbf{B}$ and the measurement matrix $\mathbf{H}$ are defined as,

$$\mathbf{B} = \begin{bmatrix} dt \\ dt \end{bmatrix} \quad and \quad \mathbf{H} = \begin{bmatrix} 1 & 0 \\ 0 & 1 \end{bmatrix}. \tag{7}$$

It should be noted that $\mathbf{H}$ is simply $\mathbf{I}$ since the measurement (i.e. detection from SiamFC) directly gives the coordinates of the centroid of the best-matched candidate block.

The two phases of Kalman filtering, namely, *prediction* and *update* phase. In the prediction phase, priori state estimate ($\hat{\mathbf{x}}_\mathbf{k}^-$) and the priori state covariance estimate ($\mathbf{P}_\mathbf{k}^-$) are calculated using the below equations:

$$\hat{\mathbf{x}}_\mathbf{k} = \mathbf{F} \hat{\mathbf{x}}_{\mathbf{k-1}} + \mathbf{B u_{k-1}}$$
$$\mathbf{P}_\mathbf{k}^- = \mathbf{F P_{k-1} F}^T + \mathbf{Q}. \tag{8}$$

In the update phase, Kamlan gain $\mathbf{K}$, posterior estimate ($\hat{\mathbf{x}}_\mathbf{k}$) and posterior estimate of state covariance ($\mathbf{P_k}$) are calculated using the following equations:

$$\mathbf{K} = \mathbf{P}_\mathbf{k}^- \mathbf{H}^T (\mathbf{H P}_\mathbf{k}^- \mathbf{H}^T + \mathbf{C})^{-1}$$
$$\hat{\mathbf{x}}_\mathbf{k} = \hat{\mathbf{x}}_\mathbf{k}^- + \mathbf{K}(\mathbf{z_k} - \mathbf{H} \hat{\mathbf{x}}_\mathbf{k}^-)$$
$$\mathbf{P_k} = (\mathbf{I} - \mathbf{KH}) \mathbf{P}_\mathbf{k}^-. \tag{9}$$

In summary, we define a reference block in the first frame and input it to the first network. Subsequent frames are input to the second network to select the best-matching candidate block. The resulting tracked output is input to the EKF as measurement and the location of the centroid is predicted using the non-linear motion model. EKF performs a correction based on the obtained prediction and measurement. The corrected block is then compared with the reference block and if it if found to be within the predefined threshold, we update the reference block.

III. Experiments

For this study, eight image sequences of the longitudinal section of the carotid artery were from healthy volunteers were collected. A linear array probe scanner that has a center frequency of 7.5MHz from Sonix RP (LA14-5/38) was used to collect the data (data used for this study were approved by the Institutional Review Board of the University of Minnesota [26, 27]). Fig. 3a represents a sample frame of the longitudinal section of the carotid artery. Multiple ROIs containing intima-media complex, as shown in Fig. 3b, were selected in each image for tracking. A total of 17 such ROIs were randomly selected across eight image sequences. It should be noted that each ROI was tracked individually through the frames as the proposed model was not designed for multi-object tracking. Multiple ROIs were selected from the first frame of the every image sequence to assess the robustness of the proposed approach.

In order to compare the proposed model, we tracked the 17 ROIs using ES-SM and SiamFC-EKF. For our initial experiments, we compared our proposed model against ES-SM as there is no ground-truth present for the selected ROIs. Since ES-SM is most commonly used algorithm from motion estimation, the tracked outputs of ES-SM reasonably substitute for ground truth. We used NCC as the cost function for the ES-SM technique. After tracking the ROIs through all the image sequences, we compared the locations of the centroid obtained by the two techniques. Root Mean Squared Error (RMSE) was computed between the two

$$g_1(k) = \begin{bmatrix} tanh(1.22(k-0.4T))(1-tanh(1.22k))sin^2\frac{\pi k}{3.5T} \\ tanh(2.07(k-0.4T))(1-tanh(2.07k))sin^2\frac{\pi k}{3.5T} \end{bmatrix}$$

$$g_2(k) = \begin{bmatrix} (1+tanh(1.22(k-T)))(1+tanh(1.22(0.4T-k)))(20-\frac{20}{T}k) \\ (1+tanh(2.07(k-T)))(1+tanh(2.07(0.4T-k)))(17-\frac{17}{T}k) \end{bmatrix}$$
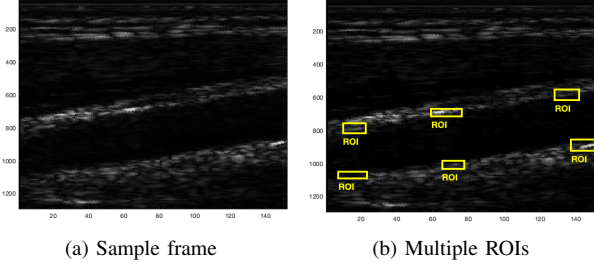
(4)

| (a) Sample frame | (b) Multiple ROIs |

Figure 3. (*a*) represents a sample frame from one of the image seuqnces and (*b*) represents multiple ROIs with intima-media complex selected for tracking.

techniques along with computational time per frame. We calculate RMSE to indicate how close are the outputs for both techniques.

IV. RESULTS AND DISCUSSION

As mentioned in the previous section, SiamFC-EKF and ES-SM were both run on 8 image sequences that contained a total of 17 ROIs. The ROIs defined in the first frame were tracked throughout the image sequence and the locations of centroid of the two techniques were compared using RMSE. In addition, the computational time per frame was also compared between the two techniques. Table 1 represents the average RMSE over all the frames between SiamFC-EKF and ES-SM. It can be seen that RMSE values in both axial and lateral directions are lesser than 1 pixel. This indicates that SiamFC-EKF is comparable to the ES-SM technique. Fig. 4 represents the axial displacement trajectory between SiamFC-EKF and ES-SM for a sample image sequence (lateral displacement trajectory is intentionally left out due to negligible arterial movement in the lateral direction). It can be visually verified that both the techniques are considerably equivalent.

Table 1. RMSE between SiamFC-EKF and ES-SM

	RMSE
Axial	0.1188
Lateral	0.3433

Table 2. Computational time per frame for SiamFC-EKF and ES-SM

	Computational time per frame
ES-SM	1.69s
SiamFC-EKF	0.33s

On the contrary, Table 2 represents the computational time per frame for both the techniques averaged over all the frames of the 17 ROIs. It can be seen that SiamFC-EKF outperforms the ES-SM technique by a substantial margin. While it takes about 1.69s on an average for ES-SM to process a frame, it only takes about 0.33s for the SiamFC-EKF to process the frame. SiamFC-EFK is, therefore, about 5 times faster than the ES-SM technique.

From the preliminary results, it can be seen that the conventional ES-SM technique could be replaced by much faster CNN-based techniques such as SiamFC-EKF without compromising on the accuracy. The intrinsic property of SiamFC-EKF allows us to input images of any size. Although the training period increasing with the increase in the input size, the computational time required during testing will remain the same [22]. On the contrary, for the iterative traditional techniques such as ES-SM the computational time increases with the size of the search region (height and width) as a function of the second order polynomial $O(height * width)$. Furthermore, it was proved that the proposed model works in real-time in our associated paper [17]. The average computational time for SiamFC-EKF was shown to be 0.33s (330ms). The total processing time (t_{total}) per frame is divided into three parts: time taken by SiamFC module (t_{SiamFC}), time taken by reference update module (t_{ru}) and time taken by the EKF module (t_{ekf}). Therefore,
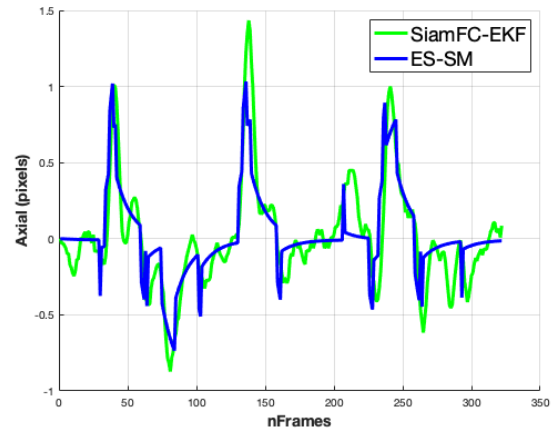

Figure 4. Axial displacement trajectory between SiamFC-EKF and EKF

$t_{total} = t_{SiamFC} + t_{ru} + t_{ekf}$. Among the three components, the detection module claims the maximum share of t_{total} with 230ms. While the reference update module (t_{ru}) takes up 19.67ms, the EKF modules consumes the rest of 80.33ms. All the experiments were run using MATLAB 2019 on a windows OS equipped with Intel i7 processor operating at a 3.4GHz with 16GB RAM. Authors in [22] also claim that the networked proposed in their paper operates at 86 fps using a GPU (NVIDIA GeForce GTX Titan X). Thus, we can safely assume that our network can also operate in real-time.

V. Conclusions

In this paper, the arterial wall motion of the carotid artery was estimated using a Siamese architecture-based convolutional neural network. The non-linear dynamics of the arterial wall motion was estimated using Van der Pol oscillator model. An EKF was used to incorporate the non-linear motion model into the proposed Siamese-based architecture. SiamFC-EKF model was compared with the traditional exhaustive search-based similarity matching technique in order to evaluate the accuracy and speed of the proposed model. Our preliminary experiments proved that SiamFC-EKF outperformed exhaustive search-based similarity matching technique in terms of computational time without compromising the accuracy. Our future work is aimed at evaluating the proposed model on an exhaustive data set with ground truth to substantiate the claim and improve the detection module.

Acknowledgements

References

[1] V. De Luca, T. Benz, S. Kondo, L. König, D. Lübke, S. Rothlübbers, O. Somphone, S. Allaire, M. L. Bell, D. Chung *et al.*, "The 2014 liver ultrasound tracking benchmark," *Physics in Medicine & Biology*, vol. 60, no. 14, p. 5571, 2015.

[2] T. Shiina, K. R. Nightingale, M. L. Palmeri, T. J. Hall, J. C. Bamber, R. G. Barr, L. Castera, B. I. Choi, Y.-H. Chou, D. Cosgrove *et al.*, "Wfumb guidelines and recommendations for clinical use of ultrasound elastography: Part 1: basic principles and terminology," *Ultrasound in Medicine & Biology*, vol. 41, no. 5, pp. 1126–1147, 2015.

[3] Y. Yue, and D. S. Khoury, and J. W. Clark, "Speckle tracking in intracardiac echocardiography for the assessment of myocardial deformation," *IEEE Transactions on Biomedical Engineering*, vol. 56, no. 2, pp. 416–425, 2008.

[4] V. De Luca, J. Banerjee, A. Hallack, S. Kondo, M. Makhinya, D. Nouri, L. Royer, A. Cifor, G. Dardenne, O. Goksel *et al.*, "Evaluation of 2d and 3d ultrasound tracking algorithms and impact on ultrasound-guided liver radiotherapy margins," *Medical Physics*, vol. 45, no. 11, pp. 4986–5003, 2018.

[5] A. J. Shepard, B. Wang, T. K. Foo, and B. P. Bednarz, "A block matching based approach with multiple simultaneous templates for the real-time 2d ultrasound tracking of liver vessels," *Medical Physics*, vol. 44, no. 11, pp. 5889–5900, 2017.

[6] T. Williamson, W. Cheung, S. K. Roberts, and S. Chauhan, "Ultrasound-based liver tracking utilizing a hybrid template/optical flow approach," *International Journal of Computer Assisted Radiology and Surgery*, vol. 13, no. 10, pp. 1605–1615, 2018.

[7] C. Shen, J. He, Y. Huang, and J. Wu, "Discriminative correlation filter network for robust landmark tracking in ultrasound guided intervention," *International Conference on Medical Image Computing and Computer-Assisted Intervention*, 2019, pp. 646—654.

[8] E. S. Ebbini, "Phase-coupled two-dimensional speckle tracking algorithm," *IEEE Transactions on Ultrasonics, Ferroelectrics, and Frequency Control*, vol. 53, no. 5, pp. 972–990, 2006.

[9] M. K. Almekkawy, Y. Adibi, F. Zheng, E. Ebbini, and M. Chirala, "Two-dimensional speckle tracking using zero phase crossing with riesz transform," *Proceedings of Meetings on Acoustics 168ASA*, vol. 22, 2014, p. 020004.

[10] M. Almekkawy and E. Ebbini, "Two-dimensional speckle tracking using parabolic polynomial expansion with riesz transform," *2017 IEEE 14th International Symposium on Biomedical Imaging (ISBI 2017)*, 2017, pp. 201–205.

[11] B. Rebholz, F. Zheng, and M. Almekkawy, "Two-dimensional iterative projection method for subsample speckle tracking of ultrasound images," *Medical & Biological Engineering & Computing*, vol. 58, no. 12, pp. 2937–2951, 2020.

[12] B. Rebholz and M. Almekkawy, "Analysis of speckle tracking methods: Correlation and rf interpolation," *2020 IEEE 4th International Conference on Image Processing, Applications and Systems (IPAS)*, 2020, pp. 120–124.

[13] B. Rebholz and M. Almekkawy, "Constrained rf level interpolation for normalized cross correlation based speckle tracking," *2020 IEEE International Ultrasonics Symposium (IUS)*, 2020, pp. 1–4.

[14] A. Dosovitskiy, P. Fischer, E. Ilg, P. Hausser, C. Hazirbas, V. Golkov, P. Van Der Smagt, D. Cremers, and T. Brox, "Flownet: Learning optical flow with convolutional networks," *Proceedings of the IEEE International Conference on Computer Vision*, 2015, pp. 2758–2766.

[15] M. G. Kibria and H. Rivaz, "Gluenet: Ultrasound elastography using convolutional neural network," *Simulation, Image Processing, and Ultrasound Systems for Assisted Diagnosis and Navigation*, 2018, pp. 21–28.

[16] S. Bharadwaj and M. Almekkawy, "Deep learning based motion tracking of ultrasound image sequences," *2020 IEEE International Ultrasonics Symposium (IUS)*, 2020, pp. 1–4.

[17] S. Bharadwaj, S. Prasad, and M. Almekkawy, "An upgraded siamese neural network for motion tracking in ultrasound image sequences," *IEEE Transactions on Ultrasonics, Ferroelectrics, and Frequency Control*, pp. 1–14, 2021.

[18] S. Bharadwaj and M. Almekkawy, "Improved siamese network for motion tracking in ultrasound images," *The Journal of the Acoustical Society of America*, vol. 149, no. 4, pp. A114–A114, 2021.

[19] S. Bharadwaj and M. Almekkawy, "Motion estimation for ultrasound image sequences using deep learning," *The Journal of the Acoustical Society of America*, vol. 148, no. 4, pp. 2487–2487, 2020.

[20] Z. Gao, Y. Li, Y. Sun, J. Yang, H. Xiong, H. Zhang, X. Liu, W. Wu, D. Liang, and S. Li, "Motion tracking of the carotid artery wall from ultrasound image sequences: a nonlinear state-space approach," *IEEE Transactions on Medical Imaging*, vol. 37, no. 1, pp. 273–283, 2017.

[21] S. Bharadwaj and M. Almekkawy, "Faster search algorithm for speckle tracking in ultrasound images," *2020 42nd Annual International Conference of the IEEE Engineering in Medicine & Biology Society (EMBC)*, 2020, pp. 2142–2146.

[22] L. Bertinetto, J. Valmadre, J. F. Henriques, A. Vedaldi, and P. H. Torr, "Fully-convolutional siamese networks for object tracking," *European Conference on Computer Vision*, 2016, pp. 850–865.

[23] G. Zahnd, L. Boussel, A. Marion, M. Durand, P. Moulin, A. Sérusclat, and D. Vray, "Measurement of two-dimensional movement parameters of the carotid artery wall for early detection of arteriosclerosis: a preliminary clinical study," *Ultrasound in Medicine & Biology*, vol. 37, no. 9, pp. 1421–1429, 2011.

[24] J. Stoitsis, S. Golemati, E. Bastouni, and K. Nikita, "A mathematical model of the mechanical deformation of the carotid artery wall and its application to clinical data," *2007 29th Annual International Conference of the IEEE Engineering in Medicine and Biology Society*, 2007, pp. 2163–2166.

[25] S. Golemati, J. S. Stoitsis, A. Gastounioti, A. C. Dimopoulos, V. Koropouli, and K. S. Nikita, "Comparison of block matching and differential methods for motion analysis of the carotid artery wall from ultrasound images," *IEEE Transactions on Information Technology in Biomedicine*, vol. 16, no. 5, pp. 852–858, 2012.

[26] Y. Wan, D. Liu, and E. S. Ebbini, "Simultaneous imaging of tissue motion and flow velocity using 2d phase-coupled speckle tracking," *2010 IEEE International Ultrasonics Symposium*, 2010, pp. 487–490.

[27] Y. Wan, D. Liu, and E. S. Ebbini, "Imaging vascular mechanics using ultrasound: Phantom and in vivo results," *2010 IEEE International Symposium on Biomedical Imaging: From Nano to Macro*, 2010, pp. 980–983.